

Unrolled Neural Networks for Constrained Optimization

Samar Hadou and Alejandro Ribeiro

Abstract—In this paper, we develop unrolled neural networks to solve constrained optimization problems, offering accelerated, learnable counterparts to dual ascent (DA) algorithms. Our framework, termed constrained dual unrolling (CDU), comprises two coupled neural networks that jointly approximate the saddle point of the Lagrangian. The primal network emulates an iterative optimizer that finds a stationary point of the Lagrangian for a given dual multiplier, sampled from an unknown distribution. The dual network generates trajectories towards the optimal multipliers across its layers while querying the primal network at each layer. Departing from standard unrolling, we induce DA dynamics by imposing primal-descent and dual-ascent constraints through constrained learning. We formulate training the two networks as a nested optimization problem and propose an alternating procedure that updates the primal and dual networks in turn, mitigating uncertainty in the multiplier distribution required for primal network training. We numerically evaluate the framework on mixed-integer quadratic programs (MIQPs) and power allocation in wireless networks. In both cases, our approach yields near-optimal near-feasible solutions and exhibits strong out-of-distribution (OOD) generalization.

Index Terms—Algorithm unrolling, constrained optimization, learning to optimize, dual ascent algorithms.

I. INTRODUCTION

Bridging the gap between model-based optimization and data-driven learning, algorithm unrolling embeds iterative solvers into neural network architectures, yielding learnable optimizers that are structured from domain-specific knowledge [1], [2]. Beyond the interpretability inherited from standard optimizers, unrolling offers accelerated convergence, with unrolled models often achieving superior performance using substantially fewer layers (i.e., iterations) than conventional iterative algorithms. While the seminal work of Greg and LeCun [1] introduced unrolling in the context of sparse coding, the approach has since achieved notable success in many applications such as computer vision [3]–[7], wireless networks [8]–[11], and medical imaging [12]–[15], among others [16]–[21].

Despite the extensive literature on unrolling, the vast majority of existing work focuses on unconstrained optimization problems. In the relatively few works that address constrained optimization, a common approach is to incorporate constraints into the training losses as penalty terms, effectively transforming the task into an unconstrained problem [21]–[23]. Another line of work considers unrolling primal-dual methods [11], [24]–[26], but typically restricts learning to a small set of scalar hyperparameters, such as step sizes, rather than learning

S Hadou and A Ribeiro are with the Department of Electrical and Systems Engineering, University of Pennsylvania, Philadelphia, PA 19104 USA (e-mail: selaraby@seas.upenn.edu; aribeiro@seas.upenn.edu).

the full algorithmic dynamics. As a result, these approaches tend to be narrowly tailored to the problem classes they were designed to address.

In this paper, we introduce constrained dual unrolling (CDU), a novel unrolling framework to solve constrained optimization problems in the dual domain. The approach employs two unrolled neural networks that collaboratively solve the dual problem, i.e., finding the saddle point of the Lagrangian function. The primal network finds a stationary point of the Lagrangian for a given multiplier, while the dual network maximizes the dual function. We cast the training problem as a nested optimization problem, where the inner level trains the primal network over a joint distribution of constrained problems and Lagrangian multipliers and the outer level trains the dual network over the distribution of problem instances. The multiplier distribution required for the inner level is not known a priori, as it depends on the sequence of multipliers generated by the forward pass of the dual network. To address this, we train our networks through an alternating scheme: the dual network first generates multipliers for training the primal network, whose solutions are then used to update the dual network. Alternating between these two steps ensures that each network is optimized against the recent output of the other.

Our method departs from traditional unrolling literature in two key aspects. First, rather than hard-coding the structure of an iterative solver, we use off-the-shelf neural networks to model the primal and dual iterates, allowing for more expressive and flexible architectures. Second, we enforce the optimization dynamics by imposing descent and ascent constraints on the outputs of the unrolled layers during training.

The first difference concerns adopting a broader interpretation of unrolling. Our unrolled networks still mimic an iterative algorithm and predict a trajectory towards the optimum across the unrolled layers. However, the architecture itself does not replicate the underlying iterative algorithm. Rather, we use a standard neural network, however shallow, as an unrolled layer. This perspective is not entirely new; similar approaches have been explored in related areas, such as optimal control [22], deep equilibrium networks [27] and plug-and-play (PnP) approaches [28], [29]. This choice is motivated by the fact that these networks can approximate continuous functions, including iterative update rules, under some regularity assumptions and with great precision [30], [31].

The second aspect tackles the lack of descent behavior of unrolled models, which our prior work has shown to be particularly susceptible to out-of-distribution (OOD) examples [32]. To address this limitation, we impose monotonic descent and ascent constraints on the output of the primal and dual

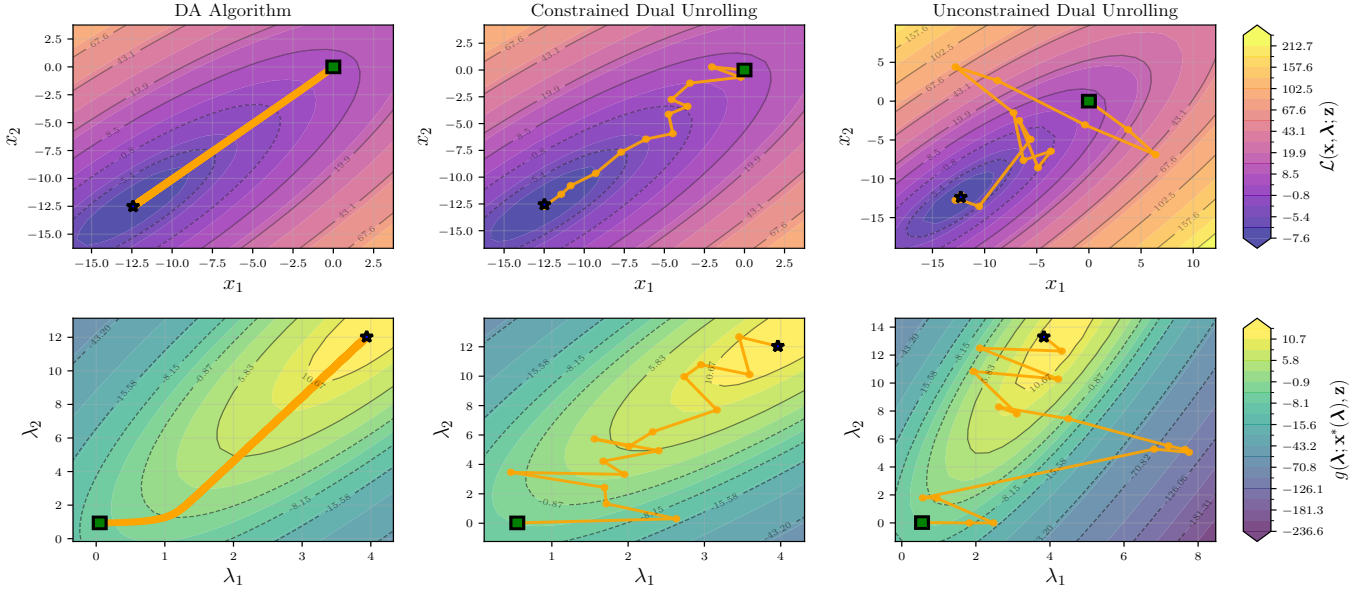


Fig. 1: Trajectories generated by (left) DA algorithm, (middle) constrained dual unrolling and (right) its unconstrained counterpart for a QP instance: (Top) primal trajectories toward the stationary point of the Lagrangian $\mathcal{L}(\cdot, \lambda; \mathbf{z})$, and (bottom) dual trajectories maximizing the dual function $g(\cdot; \mathbf{x}^*(\lambda), \mathbf{z})$. The constrained networks generate descent trajectories emulating the DA algorithm, while the unconstrained models generate random trajectories and fail to hit the optimum of the dual function (bottom right).

layers during training. Figure 1 illustrates the effect of imposing these constraints on quadratic programs (QPs). The right panels show the evolution of the Lagrangian (top) and dual (bottom) functions across the layers of primal and dual networks. The trajectories exhibit large excursions across the optimization spaces and fail to locate the maximum of the dual function as precisely as the iterative algorithm on the left. In contrast, the middle panels show that imposing the constraints yields descent and ascent trajectories toward the true solution with mild oscillations. Overall, our numerical experiments show that these descent constraints improve the final-layer performance and enhance the OOD generalization.

Last but not least, our framework is agnostic to the primal and dual architectures and the specific constrained problem being solved. In this work, we tackle mixed-integer quadratic programs (MIQP) and power allocation in wireless networks, using graph neural networks (GNNs). GNNs are particularly well-suited for these tasks, as they naturally capture the relational structure between variables and constraints, and are endowed with stability, transferability, and permutation equivariance [33]. Nevertheless, our approach generalizes to a wide range of problems and architectures.

In summary, the main contributions of this work are:

- We design a pair of primal and dual networks that interact at the layer level to solve the dual problem (Section II-B).
- We formulate the training problem as a nested optimization problem and provide an alternating training scheme that updates the two networks in turn (Section III).
- We impose descent and ascent constraints on the unrolled layers of the primal and dual networks, respectively, during training (Section III-A).
- We demonstrate the effectiveness of our approach on

two different applications, MIQP (Section IV) and power allocation problems (Section V).

II. CONSTRAINED-OPTIMIZATION UNROLLING

Consider a constrained problem that poses the task of minimizing a scalar objective function $f_0 : \mathbb{R}^n \rightarrow \mathbb{R}$, subject to m constraints,

$$P^*(\mathbf{z}) = \min_{\mathbf{x} \in \mathbb{R}^n} f_0(\mathbf{x}; \mathbf{z}) \quad \text{s.t.} \quad \mathbf{f}(\mathbf{x}; \mathbf{z}) \leq \mathbf{0}, \quad (1)$$

where $\mathbf{f} : \mathbb{R}^n \rightarrow \mathbb{R}^m$ is a vector-valued function representing the constraints, and \mathbf{z} represents a problem instance. A solution \mathbf{x} is *feasible* if it satisfies the constraints and is considered *optimal* if it minimizes the objective over all feasible solutions, i.e., $\mathbf{f}(\mathbf{x}; \mathbf{z}) \leq \mathbf{f}(\mathbf{y}; \mathbf{z})$ for all feasible \mathbf{y} .

A. Dual Formulations of Constrained Optimization

We focus on dual methods, e.g., dual ascent (DA), which address (1) via its dual formulation. The Lagrangian function $\mathcal{L} : \mathbb{R}^n \times \mathbb{R}_+^m \rightarrow \mathbb{R}$ combines the objective function with the constraints through Lagrangian multipliers $\lambda \in \mathbb{R}_+^m$,

$$\mathcal{L}(\mathbf{x}, \lambda; \mathbf{z}) = f_0(\mathbf{x}; \mathbf{z}) + \lambda^\top \mathbf{f}(\mathbf{x}; \mathbf{z}). \quad (2)$$

The dual problem is then defined as the max-min problem,

$$D^*(\mathbf{z}) = \max_{\lambda \in \mathbb{R}_+^m} \min_{\mathbf{x}} \mathcal{L}(\mathbf{x}, \lambda; \mathbf{z}), \quad (3)$$

and the duality theory affirms that $D^*(\mathbf{z}) \leq P^*(\mathbf{z})$ [34]. The equality holds under strong duality, which applies to convex problems where both the objective f_0 and the feasible set defined by \mathbf{f} are convex. Under the strong-duality assumption, the Lagrangian has a saddle point $(\mathbf{x}^*, \lambda^*)$, where \mathbf{x}^* is the

minimizer of (1) and λ^* is the maximizer of the dual problem. This motivates solving the dual problem, rather than (1), in the case of convex problems and problems with provably small duality gaps, e.g., [35].

Finding the saddle point of (3) can be recast as the nested optimization problem,

$$D^*(\mathbf{z}) = \max_{\lambda \in \mathbb{R}_+^m} g(\lambda; \mathbf{x}^*(\lambda), \mathbf{z}) := \mathcal{L}(\mathbf{x}^*(\lambda), \lambda; \mathbf{z}) \quad (4)$$

$$\text{with } \mathbf{x}^*(\lambda) \in \operatorname{argmin}_{\mathbf{x}} \mathcal{L}(\mathbf{x}, \lambda; \mathbf{z}), \quad (5)$$

where $g : \mathbb{R}_+^m \rightarrow \mathbb{R}$ is the dual function. The inner-level problem (Figure 1, top) finds the minimizer $\mathbf{x}^*(\lambda)$ of the Lagrangian function for any given λ . The outer-level problem (Figure 1, bottom) maximizes the dual function g , which is defined as the Lagrangian function evaluated at the minimizer $\mathbf{x}^*(\lambda)$. We resort to the formulation in (4)–(5) because it mirrors the dynamics of the DA algorithm.

The DA algorithm, depicted in Figure 1 (left), computes the dual optimum λ^* by repeating the following iteration,

$$\mathbf{x}_l \in \operatorname{argmin}_{\mathbf{x}} \mathcal{L}(\mathbf{x}, \lambda_l; \mathbf{z}), \quad (6)$$

$$\lambda_{l+1} = [\lambda_l + \eta \mathbf{f}(\mathbf{x}_l; \mathbf{z})]_+, \quad (7)$$

where η is a stepsize, and $[\cdot]_+$ denotes a projection onto \mathbb{R}_+^m . In each iteration, a Lagrangian stationary point \mathbf{x}_l is attained for the current dual multiplier λ_l , before a projected gradient ascent step is taken in the dual domain. The primal optimum \mathbf{x}^* is then recovered from the set $\mathbf{x}^*(\lambda^*)$.

B. Constrained-Optimization Unrolling

We design a pair of unrolled neural networks that collaboratively find the saddle point of (4)–(5). As illustrated in Figure 2 (middle), the dual network is the backbone of this design, where each dual layer evaluates the feasibility of the current iterate (cf. (7)) and returns a new estimate of the dual variable that shapes the next primal iterate (cf. (6)). Together, the primal and dual networks emulate the DA dynamics, as we describe next in more detail.

The primal network, denoted by $\Phi_P(\lambda, \mathbf{z}; \theta_P)$ and illustrated in Figure 2 (left), predicts the minimizer of the Lagrangian function with respect to its first argument for a given multiplier λ and a problem instance \mathbf{z} . The network consists of a cascade of K layers whose outputs constitute a trajectory from an initial point $\tilde{\mathbf{x}}_0$ to a minimizer of (5), i.e., $\tilde{\mathbf{x}}_K \approx \mathbf{x}^*(\lambda)$. The k -th primal layer refines the estimate $\tilde{\mathbf{x}}_{k-1}$ into

$$\tilde{\mathbf{x}}_k = \Phi_P^k(\tilde{\mathbf{x}}_{k-1}, \lambda, \mathbf{z}; \theta_P^k), \quad (8)$$

where θ_P^k is a learnable parameter, and $\theta_P = \{\theta_P^k\}_{k=1}^K$ collects all the parameters. We use the tilde notation to distinguish the intermediate estimates produced by the primal layers from other occurrences of \mathbf{x} elsewhere in the architecture and analysis. The parametrization θ_P can vary depending on the optimization problem we solve, and the training approach we propose in this paper is agnostic to that choice. As a general design principle, an unrolled layer θ_P^k may consist of a multi-layer neural network, rather than a single layer, to leverage their

expressivity. We also incorporate residual connections between unrolled layers as they naturally mimic gradient-based updates.

The dual network, denoted by $\Phi_D(\mathbf{z}; \theta_D, \theta_P)$, approximates the maximizer of the dual function $g(\lambda; \mathbf{x}^*(\lambda), \mathbf{z})$. The dual function depends on λ directly and indirectly through $\mathbf{x}^*(\lambda)$, which is provided by the primal network. This induces the dependence of dual network Φ_D on the primal parameterization θ_P . The dual network has L cascaded layers whose outputs trace a trajectory of estimates starting from an initial point λ_0 and ending at an estimate of the optimal multiplier $\lambda_L \approx \lambda^*$. The l -th dual layer is defined as

$$\lambda_l = \Phi_D^l(\lambda_{l-1}, \Phi_P(\lambda_{l-1}, \mathbf{z}; \theta_P), \mathbf{z}; \theta_D^l), \quad (9)$$

where θ_D^l is a learnable parameter and $\theta_D = \{\theta_D^l\}_{l=1}^L$. As per (9), the l -th dual layer queries the primal network for its estimate $\mathbf{x}_{l-1} := \Phi_P(\lambda_{l-1}, \mathbf{z}; \theta_P) \approx \mathbf{x}^*(\lambda_{l-1})$. Consequently, a single forward pass of the dual network triggers L forward passes of the primal network, as illustrated in Figure 2 (middle). The design of the dual parameterization is problem-dependent, and we follow the same design principles as in the primal network. However, the nonlinearity at the end of each dual layer is forced to be a relu function to ensure that the predicted Lagrangian multipliers are always nonnegative.

Finally, the solution to (1), $\mathbf{x}^* \in \mathbf{x}^*(\lambda^*)$, can be recovered by feeding the final dual estimate, $\lambda_L = \Phi_D(\mathbf{z}; \theta_D, \theta_P)$, to the primal network:

$$\mathbf{x}_L = \Phi_P(\Phi_D(\mathbf{z}; \theta_D, \theta_P), \mathbf{z}; \theta_P), \quad (10)$$

as depicted in Figure 2 (right). We distinguish the notation as follows: $\tilde{\mathbf{x}}_k$ denotes the estimate generated by the k -th internal layer of the primal network, while \mathbf{x}_l refers to the output of the primal network when queried with λ_l to approximate $\mathbf{x}^*(\lambda_l)$.

Our goal is to train the primal and dual networks such that the output of the primal network satisfies $\tilde{\mathbf{x}}_K \approx \mathbf{x}^*(\lambda)$ for any λ , and the output of the dual network satisfies $\lambda_L \approx \lambda^*$ for a given optimization problem. In addition, the predicted trajectories should follow descent and ascent dynamics with respect to the corresponding optimization variable.

III. CONSTRAINED DUAL UNROLLING

We formulate an unsupervised training problem that mirrors the dual problem in (4)–(5). We cast the training as a nested optimization problem where the deterministic objectives are replaced with statistical counterparts evaluated over a distribution of problem instances. The outer problem corresponds to training the dual network, while the inner problem trains the primal network. Formally, we define the training problem as

$$\theta_D^* \in \operatorname{argmax}_{\theta_D} \mathbb{E}[\mathcal{L}(\Phi_P(\lambda_L, \mathbf{z}; \theta_P^*), \lambda_L; \mathbf{z})], \quad (11)$$

$$\text{with } \theta_P^* \in \operatorname{argmin}_{\theta_P} \mathbb{E}[\mathcal{L}(\Phi_P(\lambda, \mathbf{z}; \theta_P), \lambda; \mathbf{z})], \quad (12)$$

where $\lambda_L = \Phi_D(\mathbf{z}; \theta_D, \theta_P^*)$ is the final output of the dual network evaluated for a problem instance \mathbf{z} .

The joint objective in (11)–(12), however, does not guarantee that the trajectories formed by the trained primal and dual

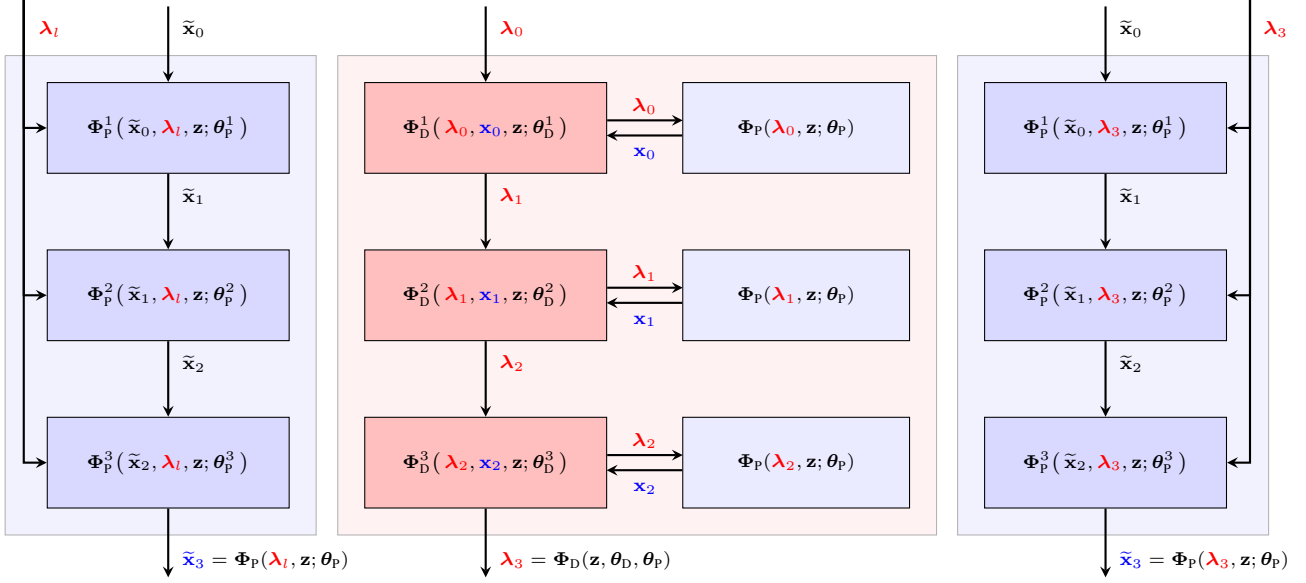


Fig. 2: Constrained-optimization unrolling in (8)–(10). (Left) The primal network with $K = 3$ unrolled layers approximates the stationary point \mathbf{x}_l for a given λ_l . (Middle) The dual network with $L = 3$ layers (red) calls the primal network (blue) at each layer, steering the iterates toward $\lambda_3 \approx \lambda^*$. (Right) The solution \mathbf{x}^* is recovered by feeding λ_3 into the primal network.

networks exhibit the descent and ascent behavior of the DA algorithm. This limitation is evident in Figure 1 (right), where the primal (top) and dual (bottom) networks generate random trajectories with large excursions before missing the maximizer of the dual function. This is because the objectives depend solely on the final outputs of the primal and dual networks without explicitly encouraging intermediate layers to follow principled optimization dynamics.

To address this, we impose descent and ascent constraints on the training objectives and reformulate the two levels as constrained training problems. Under these constraints, primal and dual networks, depicted in Figure 1 (middle), generate predominantly monotone trajectories with only mild oscillations and recover a saddle point that is substantially closer to the true optimum. For the rest of this section, we describe the constrained training paradigm that yields such descent and ascent trajectories.

A. Constrained Dual Unrolled Networks

The primal network is required to monotonically decrease the Lagrangian function across its layers. For this, we reformulate the inner problem as the constrained problem:

$$\begin{aligned} \theta_p^* \in \operatorname{argmin}_{\theta_p} \mathbb{E} \left[\mathcal{L}(\Phi_p(\lambda, z; \theta_p), \lambda; z) \right], \\ \text{s.t. } \mathbb{E} \left[\mathcal{L}(\tilde{\mathbf{x}}_k, \lambda; z) - \alpha_k \mathcal{L}(\tilde{\mathbf{x}}_{k-1}, \lambda; z) \right] \leq 0, \quad \forall k, \end{aligned} \quad (13)$$

where α_k is a design parameter controlling the descent rate and the initial value $\tilde{\mathbf{x}}_0$ is chosen randomly from a predetermined distribution, e.g., uniform. In (13), the objective function and constraints are obtained in expectation over the joint distribution of problem instances and Lagrangian multipliers. Alternatively, if the Lagrangian is differentiable with respect to \mathbf{x} , one

may enforce descent by requiring the norm of the gradient to decrease across layers, i.e., we force $\|\nabla_{\mathbf{x}} \mathcal{L}(\tilde{\mathbf{x}}_k, \lambda; z)\| \leq \alpha_k \|\nabla_{\mathbf{x}} \mathcal{L}(\tilde{\mathbf{x}}_{k-1}, \lambda; z)\|$ for all k , as previously proposed in [32]. While not entirely equivalent, since they may yield different trajectories, the two formulations promote convergence toward stationary points of the Lagrangian.

The dual network is required to ensure monotonic increase in the dual function across its layers. A key property of the dual function is its concavity, and in turn, the existence of a unique global maximum. Since we have $\mathbf{f}(\mathbf{x}^*(\lambda)) \in \partial g(\lambda)$ by Danskin’s theorem [36], we impose constraints that reduce the ℓ_2 -norm of the constraint slack $\|\mathbf{f}(\mathbf{x}_l; \cdot)\|$ across the layers as a proxy for ascending the dual function. The training of the dual network is then defined as the constrained problem:

$$\begin{aligned} \theta_D^* \in \operatorname{argmax}_{\theta_D} \mathbb{E} \left[\mathcal{L}(\Phi_p(\lambda_L, z; \theta_p^*), \lambda_L; z) \right], \\ \text{s.t. } \mathbb{E} \left[\|\mathbf{f}(\mathbf{x}_l; z)\| - \beta_l \|\mathbf{f}(\mathbf{x}_{l-1}; z)\| \right] \leq 0, \quad \forall l, \end{aligned} \quad (14)$$

where $\beta_l \in (0, 1]$ is a design parameter, λ_0 is initialized randomly, and the expectations are over a distribution of problem instances. The quantities \mathbf{x}_l , for all l , are naturally produced during the forward pass of the dual network, and therefore no additional computation is required to evaluate the constraints.

Following [32], we add Gaussian noise $\xi_k \sim \mathcal{N}(\mathbf{0}, \sigma_k^2 \mathbf{I})$ and $\xi_l \sim \mathcal{N}(\mathbf{0}, \gamma_l^2 \mathbf{I})$ to the outputs of each unrolled primal and dual layer, respectively, during training only. The noise variance decreases across layers to ensure that the final estimates are not contaminated by excessive randomness. As discussed in that work, the additive noise encourages each layer to take steps that are less dependent on the precise path taken by earlier layers. It also promotes exploration of the optimization

landscape, which, when combined with descent constraints, improves the generalizability of unrolled models.

In principle, the primal network can be trained separately over the joint problem-multiplier distribution. However, this distribution is generally unknown *a priori* as it captures the range of multipliers that the dual network may generate during execution. The nested formulation in (11)–(12) circumvents this challenge by enabling an alternating training scheme. First, the dual network is updated on the outer-level objective, producing multiplier trajectories across its layers. These multipliers are then used as training data for the primal network in the inner problem. The updated primal network subsequently generates new primal solutions that inform the next dual update. Algorithm 1 summarizes this alternating scheme. For each problem, we perform a fixed number of stochastic gradient steps before switching to the other, allowing both networks to jointly converge. This process implicitly samples from the true multiplier distribution, ensuring that each network is optimized against data generated by the current state of the other. In the following, we elaborate on these training procedures.

B. Primal Network Training

At the $(m+1)$ -th training iteration, we first consider the empirical training problem of the primal network, defined as

$$\begin{aligned} \theta_P^{(m+1)} \in \min_{\theta_P} \widehat{\mathbb{E}} \left[\mathcal{L}(\Phi_P(\lambda^{(m)}, \mathbf{z}; \theta_P), \lambda^{(m)}; \mathbf{z}) \right], \\ \text{s.t. } \widehat{\mathbb{E}} \left[\mathcal{L}(\tilde{\mathbf{x}}_k, \lambda^{(m)}; \mathbf{z}) - \alpha_k \mathcal{L}(\tilde{\mathbf{x}}_{k-1}, \lambda^{(m)}; \mathbf{z}) \right] \leq 0, \forall k, \end{aligned} \quad (15)$$

where the superscript (m) denotes the iteration index and $\widehat{\mathbb{E}}$ represents the empirical average. Equation (15) is equivalent to (13) except that the statistical average is replaced with its empirical counterpart evaluated over N problem instances, each paired with M realizations of the multipliers. To construct this dataset, for each problem instance \mathbf{z} , the dual network $\theta_D^{(m)}$ is executed with different random initializations λ_0 , and then a set of M Lagrangian multipliers is sampled from the outputs of the dual layers. These multipliers are detached from the computation graph and we do not backpropagate through them.

Problem (15) is a constrained optimization problem itself, which we solve through its dual problem [35]. We first construct the Lagrangian function using dual multipliers $\mu \in \mathbb{R}_+^K$, which we refer to as *meta* Lagrangian and *meta* multipliers to distinguish them from those associated with the original problem in (1). The meta Lagrangian function is defined as

$$\begin{aligned} \mathcal{L}_P(\theta_P, \mu) = \widehat{\mathbb{E}} \left[\mathcal{L}(\Phi_P(\lambda^{(m)}, \mathbf{z}; \theta_P), \lambda^{(m)}; \mathbf{z}) \right] \\ + \sum_{k=1}^K \mu_k \cdot \widehat{\mathbb{E}} \left[\mathcal{L}(\tilde{\mathbf{x}}_k, \lambda^{(m)}; \mathbf{z}) - \alpha_k \mathcal{L}(\tilde{\mathbf{x}}_{k-1}, \lambda^{(m)}; \mathbf{z}) \right], \end{aligned} \quad (16)$$

where μ_k is the meta multiplier associated with the k -th constraint. The corresponding dual problem is then given by

$$D_P = \max_{\mu \in \mathbb{R}_+^K} \min_{\theta_P} \mathcal{L}_P(\theta_P, \mu), \quad (17)$$

Algorithm 1 Joint Training (calls Algorithms 2 and 3)

Require: initial params θ_P, θ_D , initial meta multipliers μ, ν , training rates $\epsilon_P, \eta_P, \epsilon_D, \eta_D$, dataset \mathcal{D}_z

- 1: **for** each iteration **do**
- 2: $\theta_P, \mu \leftarrow \text{TRAINPRIMAL}(\theta_P, \theta_D, \mu, \epsilon_P, \eta_P, \mathcal{D}_z)$
- 3: $\theta_D, \nu \leftarrow \text{TRAININDUAL}(\theta_P, \theta_D, \nu, \epsilon_D, \eta_D, \mathcal{D}_z)$
- 4: **end for**
- 5: **return** θ_P, θ_D

which we solve with a primal-dual algorithm, outlined in Algorithm 2. The algorithm executes a stochastic primal-dual approach, where it constructs batches of size $N_B M$. Then, it alternates between a stochastic gradient-descent step that minimizes \mathcal{L}_P with respect to θ_P and a gradient-ascent step that maximizes it with respect to μ .

The inner problem in (17) can be viewed as a regularized problem, where the Lagrangian loss at each layer is regularized by the weight learned by the outer problem. The outer problem determines how much each layer contributes to minimizing the Lagrangian, thereby ensuring that all layers, not only the final one, actively drive the trajectory toward a stationary point and sustain monotonic descent dynamics.

C. Dual Network Training

Given the recent primal network $\theta_P^{(m+1)}$, we update the dual network through the empirical constrained problem:

$$\begin{aligned} \theta_D^{(m+1)} \in \operatorname{argmax}_{\theta_D} \widehat{\mathbb{E}} \left[\mathcal{L}(\Phi_P(\lambda_L, \mathbf{z}; \theta_P^{(m+1)}), \lambda_L; \mathbf{z}) \right], \\ \text{s.t. } \widehat{\mathbb{E}} \left[\|\mathbf{f}(\mathbf{x}_l; \mathbf{z})\| - \beta_l \|\mathbf{f}(\mathbf{x}_{l-1}; \mathbf{z})\| \right] \leq 0, \forall l, \end{aligned} \quad (18)$$

where $\widehat{\mathbb{E}}$ denotes the empirical average over N problem instances and we let $\mathbf{x}_l = \Phi_P(\lambda_l, \mathbf{z}; \theta_P^{(m+1)})$. By convention, we convert (18) into a minimization problem by negating the objective function and write the meta Lagrangian function as

$$\begin{aligned} \mathcal{L}_D(\theta_D, \nu) = -\widehat{\mathbb{E}} \left[\mathcal{L}(\Phi_P(\lambda_L, \mathbf{z}; \theta_P^{(m+1)}), \lambda_L; \mathbf{z}) \right] \\ + \sum_{l=1}^L \nu_l \cdot \widehat{\mathbb{E}} \left[\|\mathbf{f}(\mathbf{x}_l; \mathbf{z})\| - \beta_l \|\mathbf{f}(\mathbf{x}_{l-1}; \mathbf{z})\| \right], \end{aligned} \quad (19)$$

where $\nu \in \mathbb{R}_+^L$ is a vector collecting the meta multipliers associated with the constraints. Similarly to (17), the dual problem is given by

$$D_D = \max_{\nu \in \mathbb{R}_+^L} \min_{\theta_D} \mathcal{L}_D(\theta_D, \nu), \quad (20)$$

which we solve by alternating between minimization over θ_D and maximization over ν , as detailed in Algorithm 3.

It may seem circular that we replace the original convex program in (1) with the nonconvex formulations in (15) and (18), and then solve the latter with the same dual method we unroll. The rationale is computational; in many applications, (1) must be solved repeatedly for varying instances, each requiring a full run of an iterative solver. Our approach shifts this cost to an offline training process, where the original solver is

Algorithm 2 TRAINPRIMAL: Primal Network Training

Require: $\theta_P, \theta_D, \mu, \epsilon_P, \eta_P, \mathcal{D}_z$

- 1: **for** each epoch **do**
- 2: **for** each primal batch **do**
- 3: Sample a batch of N_B problem instances, $\{\mathbf{z}_{(j)}\}_{j=1}^{N_B} \sim \mathcal{D}_z$
- 4: Sample M multipliers per problem, $\{\boldsymbol{\lambda}_{(i,j)}\}_{i=1, j=1}^{M, N_B}$, from the trajectories generated by θ_D ▷ Eq. (9)
- 5: Execute the primal network to generate primal trajectories $\{\tilde{\mathbf{x}}_{k,(i,j)}\}_{k,i,j}$ ▷ Eq. (8)
- 6: Compute the empirical meta Lagrangian function,

$$\mathcal{L}_P(\theta_P, \mu) \leftarrow \frac{1}{N_B M} \sum_{j=1}^{N_B} \sum_{i=1}^M \mathcal{L}(\tilde{\mathbf{x}}_{K,(i,j)}, \boldsymbol{\lambda}_{(i,j)}; \mathbf{z}) + \sum_{k=1}^K \mu_k \cdot \left(\mathcal{L}(\tilde{\mathbf{x}}_{k,(i,j)}, \boldsymbol{\lambda}_{(i,j)}; \mathbf{z}) - \alpha_k \mathcal{L}(\tilde{\mathbf{x}}_{k-1,(i,j)}, \boldsymbol{\lambda}_{(i,j)}; \mathbf{z}) \right)$$
- 7: $\theta_P \leftarrow \theta_P - \epsilon_P \cdot \nabla_{\theta_P} \mathcal{L}_P(\theta_P, \mu)$ ▷ update the primal parametrization
- 8: $\mu \leftarrow [\mu + \eta_P \cdot \nabla_{\mu} \mathcal{L}_P(\theta_P, \mu)]_+$ ▷ update the meta Lagrangian variable
- 9: **end for**
- 10: **end for**
- 11: **return** θ_P, μ

Algorithm 3 TRAINDUAL: Dual Network Training

Require: $\theta_P, \theta_D, \nu, \epsilon_D, \eta_D, \mathcal{D}_z$

- 1: **for** each epoch **do**
- 2: **for** each dual batch **do**
- 3: Sample a batch of N_B problem instances $\{\mathbf{z}_{(i)}\}_{i=1}^{N_B} \sim \mathcal{D}_z$
- 4: Execute the dual network to generate $\{(\boldsymbol{\lambda}_{l,(i)}, \mathbf{x}_{l,(i)})\}_{l,i}$, where $\mathbf{x}_{l,(i)} = \Phi_P(\boldsymbol{\lambda}_{l,(i)}, \mathbf{z}; \theta_P)$
- 5: Compute the empirical meta Lagrangian function,

$$\mathcal{L}(\theta_D, \nu) \leftarrow \frac{-1}{N_B} \sum_{i=1}^{N_B} \mathcal{L}(\mathbf{x}_{L,(i)}, \boldsymbol{\lambda}_{L,(i)}; \mathbf{z}_{(i)}) + \sum_{l=1}^L \nu_l \cdot \left(\|\mathbf{f}(\mathbf{x}_{l,(i)}; \mathbf{z}_{(i)})\| - \beta_l \|\mathbf{f}(\mathbf{x}_{l-1,(i)}; \mathbf{z}_{(i)})\| \right)$$
- 6: $\theta_D \leftarrow \theta_D - \epsilon_D \cdot \nabla_{\theta_D} \mathcal{L}(\theta_D, \nu)$ ▷ update the dual parametrization
- 7: $\nu \leftarrow [\nu + \eta_D \cdot \nabla_{\nu} \mathcal{L}(\theta_D, \nu)]_+$ ▷ update the meta Lagrangian variable
- 8: **end for**
- 9: **end for**
- 10: **return** θ_D, ν

used only to optimize the primal and dual parameterizations. Once trained, solving (1) for a new instance reduces to a single forward pass, thereby achieving substantial reductions in online computational cost.

IV. MIXED-INTEGER QUADRATIC PROGRAMS

We consider a mixed-integer quadratic program (MIQP) with linear inequality constraints, formulated as:

$$\min_{\mathbf{x}} \quad \frac{1}{2} \mathbf{x}^\top \mathbf{P} \mathbf{x} + \mathbf{q}^\top \mathbf{x} \quad (21)$$

$$\text{s.t.} \quad \bar{\mathbf{A}} \mathbf{x} \leq \bar{\mathbf{b}}, \quad (22)$$

$$x_i \in \{-1, 1\}, \quad \forall i \in \mathcal{I}, \quad (23)$$

where $\mathbf{x} \in \mathbb{R}^n$, $\mathbf{P} \in \mathbb{R}^{n \times n}$, $\mathbf{q} \in \mathbb{R}^n$, $\bar{\mathbf{A}} \in \mathbb{R}^{m \times n}$, $\bar{\mathbf{b}} \in \mathbb{R}^m$, and \mathcal{I} is a set that contains the indices of the binary components. In (21), the objective function is convex, following the assumption that \mathbf{P} is positive semi-definite. The constraints in (22) impose linear inequalities, while (23) enforces binary values for selected components of \mathbf{x} .

Solving the MIQP in (21)–(23) is generally NP-hard due to the binary constraints, which introduce combinatorial complexity. To mitigate this issue, we resort to a convex relaxation of (23), where the binary variables are relaxed to lie in the continuous interval $[-1, 1]$. I.e., we replace $x_i \in \{-1, 1\}$ with

$-1 \leq x_i \leq 1, \quad \forall i \in \mathcal{I}$. Under this relaxation, the MIQP reduces to a convex quadratic program,

$$P^* = \min_{\mathbf{x}} \quad \frac{1}{2} \mathbf{x}^\top \mathbf{P} \mathbf{x} + \mathbf{q}^\top \mathbf{x}, \quad \text{s.t.} \quad \mathbf{A} \mathbf{x} \leq \mathbf{b}, \quad (24)$$

where $\mathbf{A} \in \mathbb{R}^{m+2|\mathcal{I}| \times n}$ and $\mathbf{b} \in \mathbb{R}^{m+2|\mathcal{I}|}$. The new constraints in (24) encode the original linear constraints (22) and the newly introduced box constraints. Specifically, we set $\mathbf{A} = [\bar{\mathbf{A}}; \mathbf{M}; -\mathbf{M}]$, where $\mathbf{M} \in \{0, 1\}^{|\mathcal{I}| \times n}$ is a selection matrix such that each row corresponds to one element in \mathcal{I} , with 1 in the column representing its index and zeros elsewhere. We also define the new constraint slack as $\mathbf{b} = [\bar{\mathbf{b}}; \mathbf{1}; \mathbf{1}]$, where $\mathbf{1}$ is a $|\mathcal{I}|$ -dimensional vector of all ones. The convex relaxation in (24) not only serves as an efficient approximation of the original MIQP, but also plays a crucial role in exact solution methods such as branch-and-bound algorithms [37], [38].

The Lagrangian function associated with the relaxed problem (24) is defined as

$$\mathcal{L}(\mathbf{x}, \boldsymbol{\lambda}) = \mathbf{x}^\top \mathbf{P} \mathbf{x} + \mathbf{q}^\top \mathbf{x} + \boldsymbol{\lambda}^\top (\mathbf{A} \mathbf{x} - \mathbf{b}), \quad (25)$$

with $\boldsymbol{\lambda} \in \mathbb{R}_+^{m+2|\mathcal{I}|}$ is the Lagrangian multiplier vector that collects the multipliers associated with each constraint. Our goal is to train a primal and a dual network that collaboratively predict the saddle point of the Lagrangian function for any instance drawn from a family of MIQP problems. Each problem instance is identified by its parameters \mathbf{P} , $\bar{\mathbf{A}}$, \mathbf{q} , $\bar{\mathbf{b}}$, and \mathcal{I} . While

the specific entries of \mathcal{I} may differ across instances, we assume that its cardinality remains fixed at $|\mathcal{I}| = r$ for all realizations.

A. GNN-based Architectures

We parametrize the primal and dual networks with two GNNs. To facilitate this, we represent the MIQP problem as a graph that captures the relationships between the optimization variables and the constraints. The graph comprises n nodes corresponding to the decision variables and $m + 2r$ nodes representing the constraints. The graph adjacency is then defined as

$$\mathbf{S} = \begin{bmatrix} \mathbf{P} & \mathbf{A}^\top \\ \mathbf{A} & \mathbf{0} \end{bmatrix}, \quad (26)$$

where \mathbf{P} and \mathbf{A} are as defined in (24). For notational convenience, and without loss of generality, we index the nodes such that the n variable nodes precede the $m + 2r$ constraint nodes in the adjacency matrix.

The core layer of GNNs consists of a graph filter followed by a nonlinearity [39]. The graph filter is defined as a polynomial function of a graph shift operator (GSO), typically represented by a matrix such as the adjacency matrix or the graph Laplacian. The output of the ℓ -th graph layer is then given by

$$\mathbf{X}_\ell = \varphi \left(\sum_{h=0}^{K_h} \mathbf{S}^h \mathbf{X}_{\ell-1} \Theta_{\ell,h} \right), \quad (27)$$

where $\Theta_{\ell,h} \in \mathbb{R}^{F_{\ell-1} \times F_\ell}$ is the set of learnable parameters, K_h represents the number of hops used in the graph filter, and φ is a nonlinear activation function. As a design convention, we treat a block of T stacked graph layers as a single unrolled layer within both the primal and dual networks. The final F_T -dimensional output of the graph block is then processed with a linear layer to generate the new estimate.

In the primal network, each unrolled layer consists of a cascade of T_P graph sub-layers. To describe the data flow through these layers, we denote by $\tilde{\mathbf{X}}_\ell^{(k)}$ the graph signal at the ℓ -th graph sub-layer of the k -th unrolled layer, where the superscript indicates the unrolled layer and the subscript denotes the graph sub-layer within it. The input to the k th unrolled layer, $\tilde{\mathbf{X}}_0^{(k)} \in \mathbb{R}^{(n+m+2r) \times 2}$, is defined as

$$\tilde{\mathbf{X}}_0^{(k)} = \begin{bmatrix} \tilde{\mathbf{x}}_{k-1} & \mathbf{q} \\ \boldsymbol{\lambda} & \mathbf{b} \end{bmatrix}, \quad (28)$$

where $\tilde{\mathbf{x}}_{k-1}$ is the output of the previous unrolled layer, and $\boldsymbol{\lambda}$, \mathbf{q} and \mathbf{b} are input data. The output of the graph block, $\tilde{\mathbf{X}}_{T_P}^{(k)} \in \mathbb{R}^{(n+m+2r) \times F_{T_P}}$, is then processed with a linear layer to predict the new estimate of the primal variable. Formally, the output of the k th unrolled layer is given by

$$\tilde{\mathbf{x}}_k = \tilde{\mathbf{x}}_{k-1} + \mathbf{M}_P \tilde{\mathbf{X}}_{T_P}^{(k)} \mathbf{W}_k + \mathbf{c}_k, \quad (29)$$

where $\mathbf{W}_k \in \mathbb{R}^{F_{T_P}}$ and $\mathbf{c}_k \in \mathbb{R}^n$ are learnable parameters. The matrix $\mathbf{M}_P \in \{0, 1\}^{n \times (n+m+2r)}$ is a selection matrix that extracts the outputs associated with the n variable nodes and excludes the outputs of the constraint nodes.

Similarly, each unrolled dual layer contains a cascade of T_D graph sub-layers. The input to the l -th unrolled dual layer

contains the recent estimates of the primal and dual variables \mathbf{x}_{l-1} and $\boldsymbol{\lambda}_{l-1}$ along with the input parameter \mathbf{q} and \mathbf{b} , i.e.,

$$\mathbf{X}_0^{(l)} = \begin{bmatrix} \mathbf{x}_{l-1} & \mathbf{q} \\ \boldsymbol{\lambda}_{l-1} & \mathbf{b} \end{bmatrix}. \quad (30)$$

The output of this graph block, $\mathbf{X}_{T_D}^{(l)} \in \mathbb{R}^{(n+m+2r) \times F_{T_D}}$, is processed with a linear layer, followed by a relu function, to generate the following estimate

$$\boldsymbol{\lambda}_l = \varphi_{\text{relu}} \left(\mathbf{y}_{l-1} + \mathbf{M}_D \mathbf{X}_{T_D}^{(l)} \mathbf{W}_l + \mathbf{c}_l \right), \quad (31)$$

where $\mathbf{W}_l \in \mathbb{R}^{F_{T_D}}$ and $\mathbf{c}_l \in \mathbb{R}^{m+2r}$ are learnable parameters—different from those used in the unrolled primal layers despite the shared notation. Moreover, the selection matrix $\mathbf{M}_D \in \{0, 1\}^{(m+2r) \times (n+m+2r)}$ chooses the values corresponding to the constraint nodes and omits the variable nodes, and the relu activation function ensures that the multipliers are nonnegative.

B. Experiment Setup

In our experiments, we consider a family of MIQP problems with $n = 80$ decision variables, $m = 45$ linear inequality constraints and $r = 10$ binary-valued variables. For each problem instance, we draw the elements of \mathbf{A} and \mathbf{q} independently from a standard normal distribution. The matrix \mathbf{P} is designed to be positive definite and the matrix \mathbf{A} is normalized by dividing its elements by its spectral norm. The vector \mathbf{b} is then evaluated as $\mathbf{Ax} + \epsilon$, with $\epsilon \sim \text{Unif}[0, 1]^n$, to ensure that each problem is feasible.

We use a primal network consisting of $K = 14$ unrolled primal layers, each composed of $T_P = 3$ graph sub-layers. The dual network mirrors this structure, also comprising $L = 14$ dual layers with the same number of graph sub-layers, i.e., $T_D = 3$. In both networks, each graph filter aggregates information from $K_h = 1$ st hop neighbors, processes $F_l = F_k = 32$ hidden features, and is followed by a tanh activation function.

Training. To train the primal network, we construct a training dataset of 400 problem instances, divided into mini-batches of $N_B = 8$ problems. At each iteration, $M = 32$ multipliers per problem are generated to evaluate the empirical meta Lagrangian in the training loss (15). Half of these multipliers are sampled from the trajectories generated by the recent dual network. The elements of the remaining multipliers are drawn independently from a uniform distribution, i.e., $\lambda_i \sim \text{Unif}[0, 1]$, with probability 0.7, and set to zero ($\lambda_i = 0$) otherwise. Training is performed with descent constraints imposed on the gradient norm of the Lagrangian, rather than on the Lagrangian value itself. For the dual network, we use a dataset of 800 problem instances, grouped in batches of $N_B = 256$. We alternate between the two networks for 400 iterations by running one epoch of primal network training (Algorithm 2) after every 15 epochs of dual network training (Algorithm 3). Each epoch consists of a full pass over the corresponding dataset. At the end of each dual epoch, we evaluate the mean constraint violation over a validation dataset of 200 problem instances, where the violation is defined as

$$\text{constraint violation} = \max\{0, f_i(\mathbf{x})\},$$

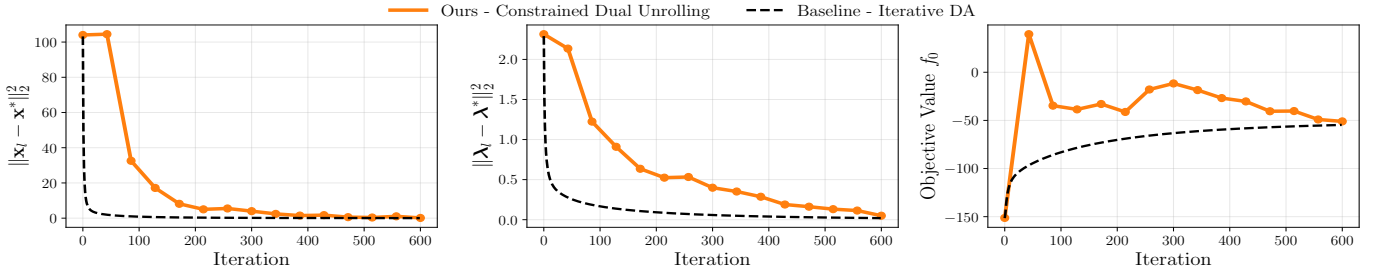


Fig. 3: Performance of constrained dual unrolling across 14 layers vs an iterative DA algorithm. (Left) The distance to the primal optimum \mathbf{x}^* , (middle) the distance to the dual optimum λ^* , and (right) the objective function (a measure of optimality). The 14-layer outputs of our method are evenly distributed across the 600 iterations for clearer visual comparison.

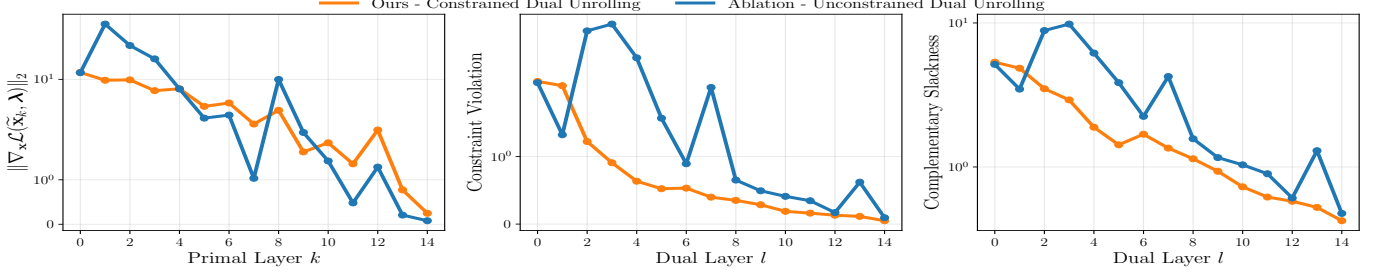


Fig. 4: Descent Guarantees. (Left) The gradient norm of the Lagrangian across the primal layers, evaluated over a test dataset of problem instances and multiplier samples. (Middle) The constraint violation across the dual layers. (Right) The complementary slackness $\lambda_L^\top \max\{\mathbf{0}, \mathbf{f}(\mathbf{x}_l)\}$ across the unrolled dual layers (a measure of feasibility). The constrained model exhibits a consistent decrease in all three quantities across layers, whereas the unconstrained model shows a more oscillatory pattern.

We then save the primal and dual models if the mean violation is within 1.5 times its recent value.

For training, we optimize the architecture parameters of the primal and dual networks using two ADAM optimizers [40] with learning rates: $\epsilon_P = 10^{-4}$ and $\epsilon_D = 7 \times 10^{-4}$. The meta Lagrangian multipliers are updated through gradient ascent with step sizes: $\eta_P = 10^{-4}$ and $\eta_D = 10^{-3}$. We share the constraint parameter $\alpha_k = 0.98$ and $\beta_l = 0.95$ across all the primal and dual layers, respectively.

Baselines. We compare the performance of our method with those of the following benchmarks:

- i. The DA algorithm, (6)–(7), with dual learning rate $\eta = 0.01$. The minimizer of the Lagrangian, \mathbf{x}_l^* , is calculated analytically by setting the gradient to zero, i.e.,

$$\mathbf{x}_l^* = -\mathbf{P}^{-1}(\mathbf{q} + \mathbf{A}^\top \lambda_l).$$

- ii. A naive GNN that consists of 42 graph layers, as in (27), with a relu activation function. The GSO is as in (26), and the input to the first layer is the vector $[\mathbf{b}; \mathbf{q}]$ that contains the constraint slack and the linear coefficient of the objective. The final graph layer is followed by a linear layer. The network is trained via a supervised paradigm to mimic the optimal solution \mathbf{x}^* , obtained by a CVXPY solver. The analysis in [41] shows that such GNN efficiently approximates the solution of (24).
- iii. Unconstrained dual unrolling, where we train the primal and dual networks without descent constraints under the same hyperparameters, except for $\epsilon_P = 10^{-3}$. This is equivalent to the approach in [42], except that we use

unsupervised training losses rather than their supervised objective.

C. Numerical Results

We evaluate the trained primal and dual networks over a test dataset of unseen 400 problem instances drawn from the same distribution as the training dataset. The optimality of the primal and dual estimates $(\mathbf{x}_l, \lambda_l)$, as well as the objective values, across the dual layers is illustrated in the three panels of Figure 3. The figure demonstrates that our constrained dual unrolling approach achieves performance comparable to that of the classical DA algorithm. However, a key advantage lies in the efficiency of our method: it reaches this level of performance in just 14 unrolled layers, as opposed to 600 iterations required by DA. This translates into a substantial reduction in computational cost at inference time, enabling rapid deployment in time-sensitive applications. This acceleration, however, comes at the expense of a computationally intensive training phase. Yet, this cost is incurred only once offline. Once trained, the unrolled networks can be deployed to solve new instances with a fixed, small number of forward passes, in stark contrast to DA, which must perform hundreds of iterative updates for each new problem. Importantly, despite this aggressive acceleration, our approach preserves the desirable descent behavior of DA.

To closely examine the role of the descent constraint, we compare the constrained model against its unconstrained counterpart and track the Lagrangian gradient norm across primal layers (left), and constraint violations across dual layers (middle)—the two quantities explicitly enforced to decrease by

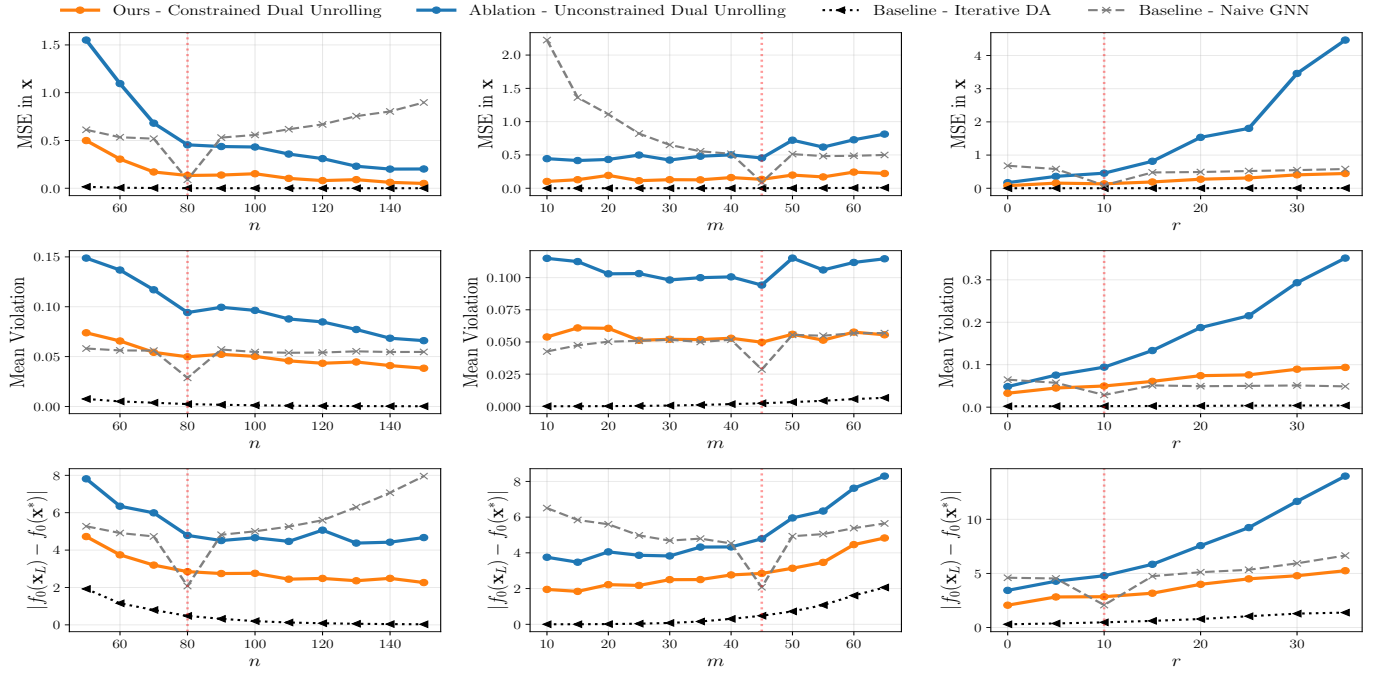


Fig. 5: Robustness under OOD problems, varying (left) the number of optimization variables n , (middle) the number of linear constraints m , and (right) the number of integer-valued variables r . The red dotted line represents the in-distribution scenario: $n = 80$, $m = 45$, and $r = 10$. Our constrained dual unrolling outperforms the learning-based benchmarks in optimality (bottom row) and feasibility (middle row) across all OOD scenarios.

the imposed constraints—alongside the complementary slackness residuals (right). As shown in Figure 4, the constrained model experiences a gradual decrease in the three quantities across the layers while the unconstrained model encounters more pronounced oscillatory behaviors. These differences are not merely aesthetic; although the overall trend for the unconstrained model still points downward, it fails to reach the same low levels of constraint violation and MSE in \mathbf{x} and λ by the constrained model. This gap is more evident in Figure 5 (the in-distribution scenario marked by a red vertical dotted line), where the constrained model attains an MSE of 0.133 in \mathbf{x} and a mean constraint violation of 0.049, compared to 0.454 and 0.094 for the unconstrained model. This indicates that descent constraints actively steer the networks toward solutions that are optimal and feasible.

Figure 5 also shows OOD experiments, where we evaluate our trained model, along with the benchmarks, on datasets generated by varying one problem parameter—either the number of variables n , constraints m , or integer-valued variables r —while keeping the others fixed. To assess the extent of distribution shift, we run the DA algorithm with the same initialization, step size, and fixed budget of 1400 iterations across all scenarios. Consequently, a degradation in the DA performance indicates that the new distribution deviates largely from the training one. This degradation is particularly pronounced when the constraint-to-variable ratio, $(m + 2r)/n$, increases.

As shown in the figure, our constrained dual unrolling consistently outperforms its unconstrained counterpart in optimality and feasibility under all OOD scenarios. The performance gap widens as the distribution shift becomes more severe—that

is, as the constraint-to-variable ratio increases, demonstrating the effectiveness of the inductive biases introduced by the descent constraints. We also observe that our constrained model surpasses the naive GNN, particularly in regimes with a low constraint-to-variable ratio. This advantage can be attributed to jointly learning the dual and primal variables: when the multiplier distribution of an OOD scenario remains close to that of the in-distribution case, the network can produce solutions that match—or even exceed—in-distribution performance. In contrast, the naive GNN does not incorporate the multipliers in its learning process and, therefore, loses these gains.

V. POWER ALLOCATION IN WIRELESS NETWORKS

Consider a network of n pairs of transmitters and receivers that share the same communication channel and cause interference to each other. The interference channel is represented by a channel state $\mathbf{H} \in \mathbb{R}^{n \times n}$ whose element h_{ij} represents the channel gain between the i -th transmitter and the j -th receiver. Under a channel state \mathbf{H} , the i -th pair transmits with power p_i and achieves a rate of

$$r_i(\mathbf{p}; \mathbf{H}) = \log \left(1 + \frac{|h_{ii}|^2 p_i}{W N_0 + \sum_{j \neq i} |h_{ji}|^2 p_j} \right), \quad (32)$$

where W is the bandwidth, N_0 is the noise power spectral density, h_{ji} is the ji -th element of \mathbf{H} , and $\mathbf{p} \in \mathbb{R}^n$ is a vector of transmit powers. The rate of the i -th user is determined by its transmit power and the interference caused by its neighboring users through their channel gains h_{ji} and transmit powers p_j .

We aim to find a policy \mathbf{p} that maximizes the sum rate of the network while forcing a subset of users \mathcal{I} to maintain a

rate of at least r_{\min} . Formally, the resource allocation problem is formulated as

$$P^* = \max_{\mathbf{p}} \mathbf{1}^\top \mathbf{r}(\mathbf{p}; \mathbf{H}) \quad (33)$$

$$\text{s.t. } r_i(\mathbf{p}; \mathbf{H}) \geq r_{\min}, \quad \forall i \in \mathcal{I}, \quad (34)$$

$$r_i(\mathbf{p}; \mathbf{H}) \geq 0, \quad \forall i \notin \mathcal{I}, \quad (35)$$

$$\mathbf{0} \leq \mathbf{p} \leq P_{\max} \cdot \mathbf{1} \quad (36)$$

where $\mathbf{1} \in \mathbb{R}^n$ is the all-one vector, and the set $\mathcal{I} \subseteq \{1, \dots, n\}$ contains the indices of the users subject to the minimum rate constraints (34). The remaining users are expected to maximize their rates, subject only to the requirement that they do not prevent the constrained users from meeting their minimum rate guarantees. Accordingly, the constraints associated with these users (35) merely enforce non-negativity, which is trivially satisfied since the rate expression in (32) is inherently non-negative. Lastly, the box constraints in (36) define the power budget P_{\max} for each user and can be implicitly enforced by applying a sigmoid activation function at the final layer of the predictive model, i.e., the primal network. Hence, we omit this constraint in the subsequent analysis.

To define the dual problem associated with (33)–(36), we first convert the problem to a minimization and construct a Lagrangian multiplier vector $\boldsymbol{\lambda} \in \mathbb{R}_+^n$ that collects the multipliers associated with the rate constraints in (34) and (35). The corresponding Lagrangian function is given by

$$\begin{aligned} \mathcal{L}(\mathbf{p}, \boldsymbol{\lambda}; \mathbf{H}) &= -\mathbf{1}^\top \mathbf{r}(\mathbf{p}; \mathbf{H}) \\ &+ \sum_{i \in \mathcal{I}} \lambda_i (r_{\min} - r_i(\mathbf{p}; \mathbf{H})) - \sum_{i \notin \mathcal{I}} \bar{\lambda}_i r_i(\mathbf{p}; \mathbf{H}), \end{aligned} \quad (37)$$

where we distinguish the multipliers associated with unconstrained users using a bar notation (i.e., $\bar{\lambda}_i$ for $i \notin \mathcal{I}$) to differentiate them from those associated with constrained users (i.e., λ_i for $i \in \mathcal{I}$). Since the constraints in (35) are trivially satisfied—as rates are nonnegative by definition—the optimal multipliers $\bar{\lambda}_i^*$ for unconstrained agents are trivially zero. For notational convenience, however, we keep these constraints in our formulation to ensure that the dimensionality of the graph signal $\boldsymbol{\lambda}$ matches that of the power signal \mathbf{p} .

Our goal is to train a primal and a dual network to predict \mathbf{p}^* and $\boldsymbol{\lambda}^*$ given a channel state matrix \mathbf{H} , drawn from a family of networks. For convenience and without loss of generality, we arrange \mathbf{H} so that the rows and columns corresponding to the constrained pairs precede those of the unconstrained pairs.

A. GNN-based Architectures

We deploy two GNNs as the underlying architectures for the primal and dual networks. Similar to (27), each graph layer consists of a graph filter followed by a nonlinearity. The output of the ℓ -th layer, $\mathbf{X}_\ell \in \mathbb{R}^{n \times F_\ell}$, is then given by

$$\mathbf{X}_\ell = \varphi \left(\sum_{h=0}^{K_h} \mathbf{H}^h \mathbf{X}_{\ell-1} \boldsymbol{\Theta}_{\ell,h} \right), \quad (38)$$

where the channel state matrix \mathbf{H} is used as a GSO, $\boldsymbol{\Theta}_{\ell,h} \in \mathbb{R}^{F_{\ell-1} \times F_\ell}$ is the set of learnable parameters, K_h represents the graph filter taps, and φ is a nonlinear activation function. Each

graph layer thus maps an $F_{\ell-1}$ -dimensional graph signal to an F_ℓ -dimensional graph signal. Following the same design convention used in the MIQP experiment, we treat a block of stacked graph layers as a single unrolled layer within both the primal and dual networks. GNNs are particularly well-suited for this setting, as the network state \mathbf{H} defines a natural graph structure, while the power allocation and Lagrangian multiplier vectors can be interpreted as graph-structured signals.

In our experiments, a primal layer consists of a cascade of T_p graph sub-layers of the form in (38). The input to the k -th primal layer, $\tilde{\mathbf{X}}_0^{(k)} \in \mathbb{R}^{n \times 3}$, stacks the recent prediction $\tilde{\mathbf{p}}_{k-1} \in \mathbb{R}^n$, the given multiplier $\boldsymbol{\lambda} \in \mathbb{R}_+^n$ and the constraint slack vector $\mathbf{s} \in \mathbb{R}^n$. The slack variable s_i is r_{\min} when $i \in \mathcal{I}$ and 0 otherwise. The output of the graph block, $\tilde{\mathbf{X}}_{T_p}^{(k)} \in \mathbb{R}^{n \times F_{T_p}}$, is processed by a nonlinear layer with parameters $\mathbf{W}_k \in \mathbb{R}^{F_{T_p}}$ and $\mathbf{c}_k \in \mathbb{R}^n$. The final output of the k -th unrolled primal layer is then given as

$$\tilde{\mathbf{p}}_k = P_{\max} \cdot \varphi_{\text{sig}} \left(\tilde{\mathbf{p}}_{k-1} + \tilde{\mathbf{X}}_{T_p}^{(k)} \mathbf{W}_k + \mathbf{c}_k \right), \quad (39)$$

where φ_{sig} the sigmoid function. The deployment of a sigmoid function ensures that $\tilde{\mathbf{p}}_k$ satisfies the power constraints in (36).

Similarly, each dual layer contains T_d cascaded graph sub-layers, followed by a nonlinear layer. The input to the l -th dual block, $\mathbf{X}_0^{(l)} \in \mathbb{R}^{n \times 3}$, is constructed by stacking the recent predictions \mathbf{p}_{l-1} and $\boldsymbol{\lambda}_{l-1}$ and the slack vector. The output of the l -th layer, $\mathbf{X}_{T_d}^{(l)} \in \mathbb{R}^{n \times F_{T_d}}$, is expressed as

$$\boldsymbol{\lambda}_l = \varphi_{\text{relu}} \left(\boldsymbol{\lambda}_{l-1} + \mathbf{m} \odot \left(\mathbf{X}_{T_d}^{(l)} \mathbf{W}_l + \mathbf{c}_l \right) \right), \quad (40)$$

where $\mathbf{W}_l \in \mathbb{R}^{F_{T_d}}$ and $\mathbf{c}_l \in \mathbb{R}^n$ are the learnable parameters of the nonlinear layer and φ_{relu} is the relu function. For notational simplicity, we use the same symbols for the nonlinear layer parameters in both the primal and dual networks, though they are trained independently. The binary mask vector $\mathbf{m} \in \{0, 1\}^n$ is defined such that $m_i = 1$ when $i \in \mathcal{I}$ and 0 otherwise. The Hadamard product ensures that the multipliers corresponding to the unconstrained agents are always set to zero, while the relu function guarantees that the multipliers are always nonnegative.

B. Experiment Setup

In our numerical experiments, we consider networks of $n = 100$ pairs of transmitters and receivers, deployed over a $1500 \times 1500 \text{ m}^2$ area. The transmitters are placed randomly, and each receiver is positioned at a distance between 20 and 60 meters from its associated transmitter. The channel state matrix represents large-scale fading that follows a dual-slope path-loss model similar to [43], combined with 7dB log-normal shadowing. We set the maximum transmit power to $P_{\max} = 0 \text{ dBm}$, the bandwidth to $W = 20 \text{ MHz}$ and the noise spectral density to $N_0 = -174 \text{ dBm/Hz}$. In each network realization, 50% of the transmitter-receiver pairs are randomly selected to be constrained, i.e., required to maintain a minimum rate of $r_{\min} = 1.5 \text{ bps/Hz}$.

We deploy a primal network that consists of $K = 4$ unrolled primal layers, each comprising $T_p = 3$ graph sub-layers and a dual network that consists of $L = 6$ dual layers, each also containing $T_d = 3$ graph sub-layers. In both networks, each

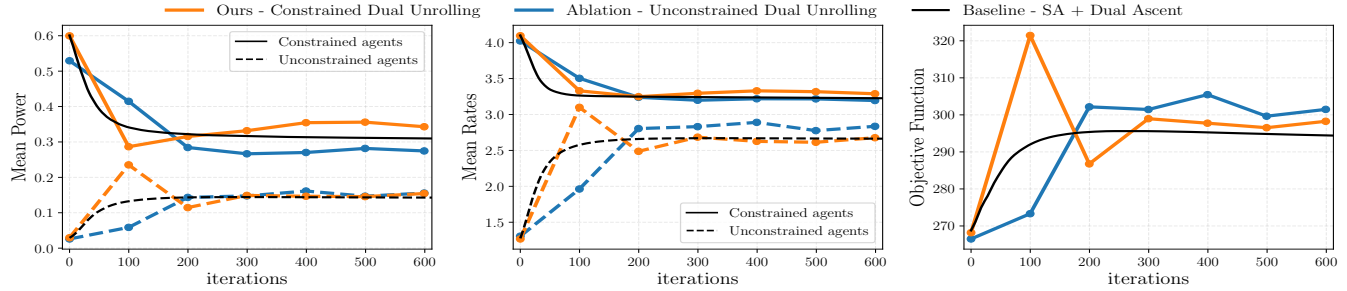


Fig. 6: Comparison of mean power, rate and constraint violation of three iterative algorithms: Constrained Dual Unrolling (ours), its unconstrained counterpart, and state-augmented dual ascent. The 6-layer outputs of dual unrolling methods are evenly distributed across the 600 iterations for clearer visual comparison. Our constrained dual unrolled networks achieve comparative performance to that of dual ascent in much fewer steps.

graph layer aggregates information from $K_h = 2$ -hop neighbors, maintains $F_l = F_k = 64$ hidden features across all intermediate layers, and deploys a leaky relu activation function.

Training. For training the primal network, we use a dataset of 512 channel state networks divided into mini-batches of a single network. At each iteration, the recent dual network is used to generate multiplier trajectories from which we select 32 samples per network realization. We augment this set with 64 samples drawn from a uniform distribution $\text{Unif}[0, 1]$ and additional 32 samples drawn from trajectories made by a classical dual ascent algorithm (the first benchmark below). For training the dual network, we use a dataset of 2048 channel state networks divided into batches of 256 graphs. The initial multipliers λ_0 are initialized such that entries corresponding to constrained users are sampled from a uniform distribution $\text{Unif}[0, 10]$, while all others are set to zero. In each iteration of our joint training scheme, we perform one epoch of primal network training (Algorithm 2) for every 5 epochs of dual network training (Algorithm 3). We alternate between training the two networks for 2000 iterations.

In training both networks, we use ADAM optimizers to update the primal and dual parameterizations with learning rates of $\epsilon_p = 10^{-4}$ and $\epsilon_d = 10^{-5}$, respectively. The meta multipliers are updated through gradient ascent with stepsizes $\eta_p = 10^{-3}$, and $\eta_d = 10^{-3}$. We share the constraint parameter $\alpha_k = 1.05$ and $\beta_l = 0.8$ across all the primal and dual layers.

Benchmarks. We compare the performance of our constrained dual unrolling with the following benchmarks over a testset of 128 channel state networks:

- State-augmentation (SA) paired with dual dynamics [44], where we use the trained primal network to predict the optimal power allocation $\mathbf{p}^*(\lambda_l)$ for the most recent multiplier λ_l and then update the multipliers using a classical gradient ascent algorithm. The iterative update is

$$\begin{aligned} \mathbf{p}_l &= \Phi_p(\lambda_l, \mathbf{H}; \theta_p^*), \\ \lambda_{l+1} &= [\lambda_l + \eta \mathbf{f}(\mathbf{p}_l; \mathbf{H})]_+, \end{aligned}$$

where \mathbf{f} combines the rate constraints in (34) and (35). We set the stepsize to $\eta = 0.05$.

- A naive GNN, consisting of 12 graph layers structured as in (38), trained to predict the optimal power allocation

- Unconstrained dual unrolling, where we train the same primal and dual architectures under identical hyperparameters, but without the descent constraints.
- A full-power policy, where all agents transmit with their maximum power P_{\max} , regardless of the constraints or the channel condition.

C. Numerical Results and Discussions

Figure 6 illustrates the iterative behavior of our constrained dual unrolling. As shown in the figure, our method follows the rate and power trajectories generated by the iterative SA method for both constrained and unconstrained users, achieving comparable performance in significantly fewer iterations. Specifically, our dual unrolling methods reach near-optimal solutions in just 6 unrolled layers compared to 600 iterations required by the iterative method. It is important to note that both methods use the same primal network, which estimates the Lagrangian minimizer $\mathbf{p}_l \approx \mathbf{p}^*(\lambda_l)$ for each multiplier λ_l . The reduction in iterations, therefore, stems from approximating the dual updates with a forward pass of the dual network. This learned approximation enables substantial acceleration while preserving feasibility and optimality.

In an ablation study, we train the same primal and dual networks without descent constraints to assess their impact on performance. Figure 7 shows that our model preserves descent behavior across the primal and dual layers, whereas the unconstrained one fails to do so. Consistent with the MIQP example, this failure to descend results in poorer performance at the final layer. This is evidenced by a higher mean violation (0.153) compared to the constrained case (0.06) and more frequent constraint violations in general, indicated by a larger area to the left of r_{\min} in the rate histogram (Figure 8-left). The right panel of this figure further reveals a gap in the histogram of predicted Lagrangian multipliers. The unconstrained model predicts zero multipliers more frequently. A zero multiplier implies that the corresponding constraint does not affect the optimality of the solution; when predicted incorrectly, it leads the model to ignore active constraints, resulting in suboptimal solutions.

To examine the OOD performance, we test our model on datasets generated by varying a single parameter—either the

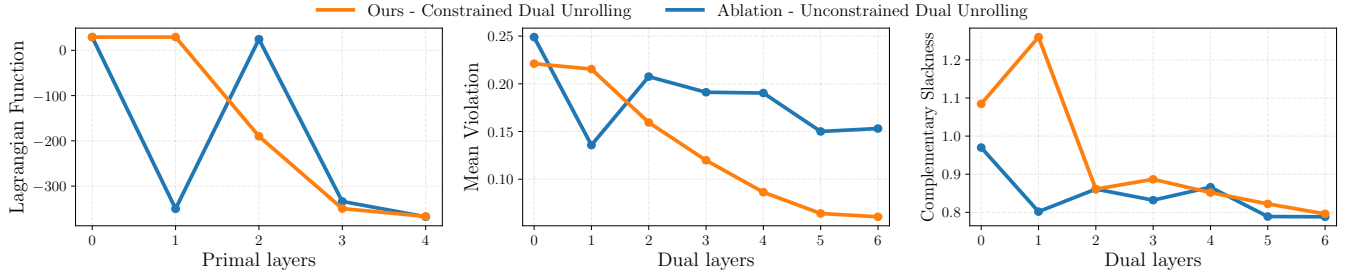


Fig. 7: Descent Guarantees. (Left) The Lagrangian function across the unrolled primal layers, evaluated over test dataset of problem instances and multiplier samples. (Middle) The constraint violation across the unrolled dual layers. (Right) The complementary slackness $\lambda_L^\top \max\{\mathbf{0}, \mathbf{f}(\mathbf{x}_L)\}$ across the unrolled dual layers. Our constrained model preserves a descent behavior over the unrolled layers, in contrast to the unconstrained model.

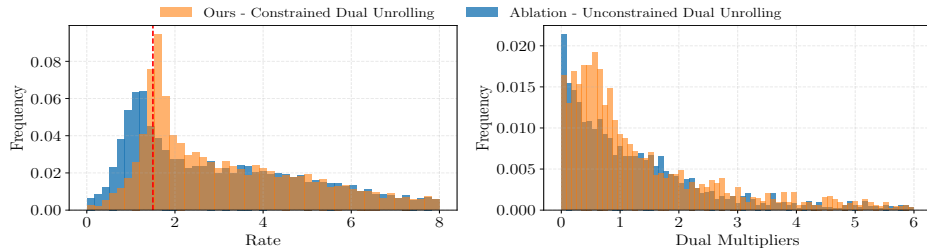


Fig. 8: Performance at the last layer. Histograms of achieved rates by constrained agents (left) and predicted dual multipliers, truncated at 6 (right). The red dashed line shows the minimum rate requirement $r_{\min} = 1.5$ for constrained agents. The unconstrained model exhibits more frequent constraint violations (the area to the left of the red dotted line).

constraint level r_{\min} , the network size n , or the constrained-agent percentage. As shown in Figure 9, our constrained dual unrolling outperforms both its unconstrained counterpart and the naive GNN across all OOD settings. The figure also shows that the performance gap widens as the constraints become harder to satisfy. This occurs either when the constraint level increases or when the number of agents grows, which leads to higher interference as the average inter-agent distance decreases. This can be attributed to the descent dynamics that is encoded in our model. Since the unconstrained model lacks this descent inductive bias, it achieves performance close to the naive GNN, which remains suboptimal due to its supervised training that does not account for the constraints [45]. Compared to the iterative SA algorithm, our constrained dual unrolling introduces errors in the regimes of harder constraints, which is expected given the mismatch in the multiplier distributions.

VI. CONCLUSIONS

This paper introduced an unrolling-based framework for constrained optimization that jointly trains a pair of unrolled networks to find the saddle point of the Lagrangian function. By imposing monotone descent and ascent constraints, our method embeds optimization-dynamics-inspired inductive biases into the unrolled networks. Extensive experiments on MIQP and wireless power allocation show that these constraints deliver strong OOD performance compared to unconstrained unrolling and supervised architectures. Descent- and ascent-driven unrolling offers a principled path to neural networks that solve

optimization problems reliably, even far beyond their training distribution.

REFERENCES

- [1] K. Gregor and Y. LeCun, “Learning fast approximations of sparse coding,” in *Proceedings of the 27th International Conference on Machine Learning, ICML’10*, pp. 399–406, June 2010.
- [2] V. Monga, Y. Li, and Y. C. Eldar, “Algorithm unrolling: Interpretable, efficient deep learning for signal and image processing,” *IEEE Signal Processing Magazine*, vol. 38, pp. 18–44, Mar. 2021.
- [3] K. Zhang, L. V. Gool, and R. Timofte, “Deep unfolding network for image super-resolution,” in *Proceedings of the IEEE/CVF conference on computer vision and pattern recognition*, pp. 3217–3226, 2020.
- [4] X. Wei, H. van Gorp, L. Gonzalez-Carabarin, D. Freedman, Y. C. Eldar, and R. J. G. van Sloun, “Deep unfolding with normalizing flow priors for inverse problems,” *IEEE Transactions on Signal Processing*, vol. 70, pp. 2962–2971, 2022.
- [5] C. Mou, Q. Wang, and J. Zhang, “Deep generalized unfolding networks for image restoration,” in *Proceedings of the IEEE/CVF Conference on Computer Vision and Pattern Recognition*, pp. 17399–17410, 2022.
- [6] Y. Li, M. Tofiqhi, J. Geng, V. Monga, and Y. C. Eldar, “Efficient and interpretable deep blind image deblurring via algorithm unrolling,” *IEEE Transactions on Computational Imaging*, vol. 6, pp. 666–681, 2020.
- [7] P. Qiao, S. Liu, T. Sun, K. Yang, and Y. Dou, “Towards vision transformer unrolling fixed-point algorithm: a case study on image restoration,” *arXiv preprint arXiv:2301.12332*, 2023.
- [8] Q. Hu, Y. Cai, Q. Shi, K. Xu, G. Yu, and Z. Ding, “Iterative algorithm induced deep-unfolding neural networks: Precoding design for multiuser MIMO systems,” *IEEE Transactions on Wireless Communications*, vol. 20, no. 2, pp. 1394–1410, 2020.
- [9] A. Chowdhury, G. Verma, C. Rao, A. Swami, and S. Segarra, “Unfolding WMMSE using graph neural networks for efficient power allocation,” *IEEE Transactions on Wireless Communications*, vol. 20, no. 9, pp. 6004–6017, 2021.
- [10] L. Schynol and M. Pesavento, “Coordinated sum-rate maximization in multicell MU-MIMO with deep unrolling,” *IEEE Journal on Selected Areas in Communications*, vol. 41, no. 4, pp. 1120–1134, 2023.

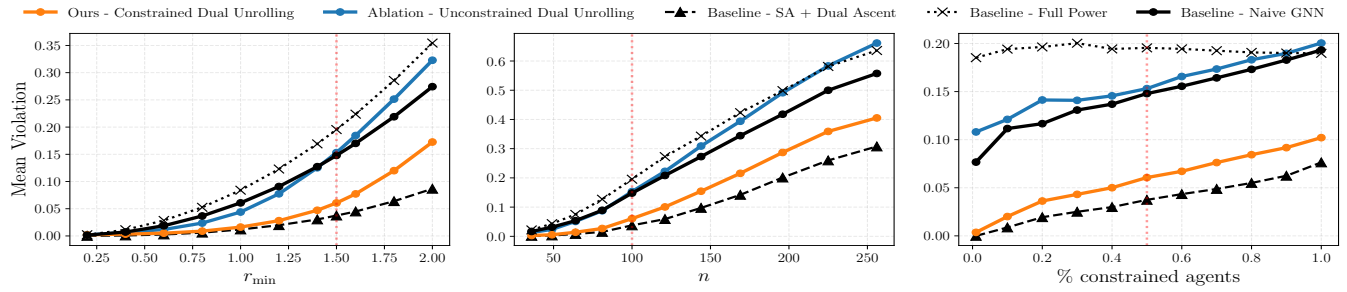


Fig. 9: Robustness under OOD problems, varying (left) the constraint level r_{\min} , (middle) the network size n , and (right) the percentage of constrained agents. The red dotted line represents the in-distribution scenario: $r_{\min} = 1.5$, $n = 100$, and 50% constrained agents. In all settings, constrained dual unrolling beats the unconstrained model and the naive GNN.

[11] J. Zhang, C. Masouros, F. Liu, Y. Huang, and A. L. Swindlehurst, “Low-complexity joint radar-communication beamforming: From optimization to deep unfolding,” *IEEE Journal of Selected Topics in Signal Processing*, pp. 1–16, 2025.

[12] P. Wang, L. Wang, G. Qu, X. Wang, Y. Zhang, and X. Yuan, “Proximal algorithm unrolling: Flexible and efficient reconstruction networks for single-pixel imaging,” in *Proceedings of the Computer Vision and Pattern Recognition Conference*, pp. 411–421, 2025.

[13] Y. Li, O. Bar-Shira, V. Monga, and Y. C. Eldar, “Deep algorithm unrolling for biomedical imaging,” *arXiv preprint arXiv:2108.06637*, 2021.

[14] N. Chennakeshava, T. S. Stevens, F. J. de Brujin, A. Hancock, M. Pekar, Y. C. Eldar, M. Mischi, and R. J. van Sloun, “Deep proximal unfolding for image recovery from under-sampled channel data in intravascular ultrasound,” in *ICASSP 2022-2022 IEEE International Conference on Acoustics, Speech and Signal Processing (ICASSP)*, pp. 1221–1225, IEEE, 2022.

[15] H. Wang, Y. Li, H. Zhang, D. Meng, and Y. Zheng, “InDuDoNet+: A deep unfolding dual domain network for metal artifact reduction in ct images,” *Medical Image Analysis*, vol. 85, p. 102729, 2023.

[16] J. R. Hershey, J. L. Roux, and F. Weninger, “Deep unfolding: Model-based inspiration of novel deep architectures,” *arXiv preprint arXiv:1409.2574*, 2014.

[17] R. Nasser, Y. C. Eldar, and R. Sharan, “Deep unfolding for non-negative matrix factorization with application to mutational signature analysis,” *Journal of Computational Biology*, vol. 29, no. 1, pp. 45–55, 2022.

[18] C. Liu, G. Leus, and E. Isufi, “Unrolling of simplicial elasticnet for edge flow signal reconstruction,” *IEEE Open Journal of Signal Processing*, pp. 1–9, 2023.

[19] N. Arab, Y. Mhiri, I. Vin, M. N. El Korso, and P. Larzabal, “Unrolled expectation maximization algorithm for radio interferometric imaging in presence of non gaussian interferences,” *Signal Processing*, p. 110035, 2025.

[20] S. Ravi and H. Larochelle, “Optimization as a model for few-shot learning,” in *International Conference on Learning Representations*, 2016.

[21] S. Hadou, N. NaderiAlizadeh, and A. Ribeiro, “Stochastic unrolled federated learning,” *arXiv preprint arXiv:2305.15371*, 2023.

[22] M. Kishida and M. Ogura, “Temporal deep unfolding for constrained nonlinear stochastic optimal control,” *IET Control Theory & Applications*, vol. 16, no. 2, pp. 139–150, 2022.

[23] C. Bertocchi, E. Chouzenoux, M.-C. Corbineau, J.-C. Pesquet, and M. Prato, “Deep unfolding of a proximal interior point method for image restoration,” *Inverse Problems*, vol. 36, no. 3, p. 034005, 2020.

[24] M. Nagahama, K. Yamada, Y. Tanaka, S. H. Chan, and Y. C. Eldar, “Graph signal restoration using nested deep algorithm unrolling,” *IEEE transactions on signal processing*, vol. 70, pp. 3296–3311, 2022.

[25] J. Yang, A. Li, X. Liao, and C. Masouros, “ADMM-SLPNet: A model-driven deep learning framework for symbol-level precoding,” *IEEE Transactions on Vehicular Technology*, vol. 73, no. 1, pp. 1376–1381, 2024.

[26] B. Li, L. Yang, Y. Chen, S. Wang, H. Mao, Q. Chen, Y. Ma, A. Wang, T. Ding, J. Tang, et al., “PDHG-unrolled learning-to-optimize method for large-scale linear programming,” in *Proceedings of the 41th International Conference on Machine Learning*, pp. 29164–29180, PMLR, 2024.

[27] S. Bai, J. Z. Kolter, and V. Koltun, “Deep equilibrium models,” *Advances in neural information processing systems*, vol. 32, 2019.

[28] E. Ryu, J. Liu, S. Wang, X. Chen, Z. Wang, and W. Yin, “Plug-and-play methods provably converge with properly trained denoisers,” in *Proceedings of the 36th International Conference on Machine Learning*, vol. 97, pp. 5546–5557, PMLR, 2019.

[29] A. Graikos, N. Malkin, N. Jojic, and D. Samaras, “Diffusion models as plug-and-play priors,” *Advances in Neural Information Processing Systems*, vol. 35, pp. 14715–14728, 2022.

[30] Z. Lu, H. Pu, F. Wang, Z. Hu, and L. Wang, “The expressive power of neural networks: A view from the width,” *Advances in neural information processing systems*, vol. 30, 2017.

[31] D. Yarotsky, “Error bounds for approximations with deep relu networks,” *Neural networks*, vol. 94, pp. 103–114, 2017.

[32] S. Hadou, N. NaderiAlizadeh, and A. Ribeiro, “Robust stochastically-descending unrolled networks,” *IEEE Transactions on Signal Processing*, vol. 72, pp. 5484–5499, 2024.

[33] L. Ruiz, L. Chamón, and A. Ribeiro, “Graphon neural networks and the transferability of graph neural networks,” in *Advances in Neural Information Processing Systems*, pp. 1702–1712, Curran Associates, Inc., 2020.

[34] S. P. Boyd and L. Vandenberghe, *Convex optimization*. Cambridge university press, 2004.

[35] L. F. Chamón, S. Paternain, M. Calvo-Fullana, and A. Ribeiro, “Constrained learning with non-convex losses,” *IEEE Transactions on Information Theory*, 2022.

[36] D. P. Bertsekas, “Nonlinear programming,” *Journal of the Operational Research Society*, vol. 48, no. 3, pp. 334–334, 1997.

[37] S. Boyd and J. Mattingley, “Branch and bound methods,” *Notes for EE364b, Stanford University*, vol. 2006, p. 07, 2007.

[38] E. L. Lawler and D. E. Wood, “Branch-and-bound methods: A survey,” *Operations research*, vol. 14, no. 4, pp. 699–719, 1966.

[39] F. Gama, E. Isufi, G. Leus, and A. Ribeiro, “Graphs, convolutions, and neural networks: From graph filters to graph neural networks,” *IEEE Signal Processing Magazine*, vol. 37, pp. 128–138, Nov. 2020.

[40] D. P. Kingma and J. Ba, “ADAM: A method for stochastic optimization,” *arXiv preprint arXiv:1412.6980*, 2014.

[41] Z. Chen, X. Chen, J. Liu, X. Wang, and W. Yin, “Expressive power of graph neural networks for (mixed-integer) quadratic programs,” in *Proceedings of the 42nd International Conference on Machine Learning*, pp. 1–32, 2025.

[42] S. Park and P. Van Hentenryck, “Self-supervised primal-dual learning for constrained optimization,” in *Proceedings of the AAAI Conference on Artificial Intelligence*, vol. 37, pp. 4052–4060, Jun. 2023.

[43] X. Zhang and J. G. Andrews, “Downlink cellular network analysis with multi-slope path loss models,” *IEEE Transactions on Communications*, vol. 63, no. 5, pp. 1881–1894, 2015.

[44] N. NaderiAlizadeh, M. Eisen, and A. Ribeiro, “State-augmented learnable algorithms for resource management in wireless networks,” *IEEE Transactions on Signal Processing*, vol. 70, pp. 5898–5912, 2022.

[45] Y. B. Uslu, S. Hadou, S. S. Bidokhti, and A. Ribeiro, “Generative diffusion models for resource allocation in wireless networks,” *arXiv preprint arXiv:2504.20277*, 2025.